RE-SHAPING HYSTERETIC BEHAVIOUR - SPECTRAL ANALYSIS AND DESIGN EQUATIONS FOR SEMI-ACTIVE STRUCTURES

Geoffrey W. Rodgers[1], John B. Mander[2], J. Geoffrey Chase[1], Kerry J. Mulligan[1], Bruce L. Deam[2] and Athol Carr[2]

Abstract

Semi-active dampers offer significant capability to reduce dynamic wind and seismic structural response. A novel resetable device with independent valve control laws that enables semi-active re-shaping of the overall structural hysteretic behaviour has been recently developed, and a one-fifth scale prototype experimentally validated. This research statistically analyses three methods of re-shaping structural hysteretic dynamics in a performance-based seismic design context. Displacement, structural force, and total base-shear response reduction factor spectra are obtained for suites of ground motions from the SAC project. Results indicate that the reduction factors are suite invariant. Resisting all motion adds damping in all four quadrants and showed 40-60% reductions in the structural force and displacement at the cost of a 20-60% increase in total base-shear. Resisting only motion away from equilibrium adds damping in quadrants 1 and 3, and provides reductions of 20-40%, with a 20-50% increase in total base-shear. However, only resisting motion towards equilibrium adds damping in quadrants 2 and 4 only, for which the structural responses *and* total base-shear are reduced 20-40%. The spectral analysis results are used to create empirical reduction factor equations suitable for use in performance based design methods, creating an avenue for designing these devices into structural applications. Overall, the reductions in both response and base-shear indicate the potential appeal of this semi-active

[1]Dept. of Mechanical Engineering, University of Canterbury, Christchurch, New Zealand
[2]Dept of Civil Engineering, University of Canterbury, Christchurch, New Zealand

hysteresis sculpting approach for seismic retrofit applications — largely due to the reduction of the structural force and overturning demands on the foundation system.

1.0 Introduction

Semi-active control is emerging as an effective method of mitigating structural damage from large environmental loads, such as wind loading and seismic excitation. It has two main benefits over active and passive solutions. First, a large power/energy supply is not required for significant reduction in response. Second, semi-active systems provide the broad range of control that a tuned passive system cannot, making them better able to respond to changes in structural behaviour due to non-linearity, damage or degradation over time. Semi-active systems are also strictly dissipative and do not add energy to the structural system, guaranteeing stability with careful implementation [1]

Because semi-active systems utilise the building motion to generate resistive forces, semi-active devices focus on managing these forces to dissipate energy in a controlled manner. It is well known that semi-active systems can dissipate significant energy and mitigate damage during seismic events, and recent research has examined re-shaping of hysteretic behaviour [2]. However, such research has not extended to investigating the relative effects of different control laws on structural response, nor has it quantified that impact statistically over suites of ground motions. Hence, there has been no examination of how to readily incorporate such novel semi-active systems into performance based design methodologies.

Semi-active devices are particularly suitable in situations where the device may not be required to be active for extended periods of time [3]. The potential of many classes of semi-active devices and methods, including variable stiffness and variable damping classes, to mitigate damage during seismic events is well documented [4-6]. This research investigates variable stiffness resetable devices where instead of altering the damping of the system, they alter the stiffness with the stored energy being released as the working fluid reverts to its initial pressure on resetting. This resetting gives rise to discontinuous jumps in the device stiffness. Thus, they are a stiffness based device that are used to dissipate stored restoring force energy.

Semi-active resetable devices show significant promise in their ability to dissipate energy and reduce seismic structural response, but are still in their infancy. Although semi-active systems may inherently raise reliability questions, regular inspection and preventative maintenance should ensure correct operation. The small power sources required for a semi-active system make them largely, if not entirely, independent of mains power and consequently unaffected by power shortages during an earthquake. Semi-active damping via resetable devices also offers the unique opportunity to sculpt or re-shape the resulting structural hysteresis loop to meet design needs, enabled by the ability to actively control the device valve and reset times. For example, given a sinusoidal response, a typical viscously damped, linear structure has the hysteresis loop definitions schematically shown in Figure 1a, where the linear force deflection response is added to the circular force-deflection response due to viscous damping to create the well-known overall hysteresis loop. Figure 1b shows the same behaviour for a simple resetable device where all stored energy is released at the peak of each sine-wave cycle and all other motion is resisted [7].

This form is denoted a “1-4 device” as it provides damping in all four quadrants. A stiff damper will dissipate significant energy. However, the resulting base-shear force is increased. If the control law is changed such that only motion *towards* the zero position (from the peak values) is resisted, the force-deflection curves that result are shown in Figure 1d. In this case, the semi-active resetable damper force actually reduces the base-shear demand by providing damping forces only in quadrants 2 and 4; this is denoted a “2-4 device”. Figure 1c shows a damper that resists motion only away from equilibrium, also increases base shear, and is denoted a “1-3 device”.

Although earthquake records are random signals and vary significantly from the harmonic response shown in Figure 1, the control implementation does not change. The only feedback measurement required for implementation is displacement information to determine position and velocity, defining the current quadrant of the displacement-velocity plot, and consequently defining the required valve position. The sampling rate is of importance for implementation, but a sampling rate of 1-2kHz is easily achievable with modern devices and allows a relatively quite simple practical implementation with modern electronics [8-11]. Hence, the fundamental systems are simple and the analyses presented here are quite general.

Overall, all three forms of resetable device enable the opportunity to re-shape and customise the overall structural hysteretic behaviour, while also providing supplemental damping to minimise structural response. Hence, Figures 1b-d show the fundamental methods by which semi-active hysteretic damping can be re-shaped with these devices. More complex patterns and control laws

may also have potential. Note that these methods are enabled by the independent control of the device valves, but could be generalised to similar viscous dampers to add further oversight of the resulting shape of the hysteretical behaviour.

This paper investigates the relative effect of the three different resetable control laws in Figures 1b-d, with their corresponding hysteretic behaviour, on structural response due to seismic excitation. When considering the effect of the additional resetable device stiffness on the structure, it is important to consider several factors. These factors include what period in a spectral response analysis shows the greatest change in response, and how to relate the non-linear resetable device stiffness, and corresponding effect on structural response, to known design guidelines. As such, the approach to the analysis presented is based around structural response spectra, as they provide a suitable way to synthesize all of these factors.

2.0 Device Dynamics

The only device control mechanism for a semi-active resetable device is the activation of the valves with a reset time of approximately 20 ms [1, 4]. The valve dynamics are more rapid than the dynamic response of most structural systems; therefore they interact only minimally with the structure. Hence, the semi-active device merely adds a non-linear stiffness to the structure. More specifically, instead of altering the damping of the structure, resetable devices are fundamentally hydraulic spring elements in which the un-stretched spring length can be reset to obtain maximum energy dissipation from the structural system [3]. Energy is stored by compressing the working fluid as a piston is displaced. When the piston reaches its maximum displaced position,

the stored energy is also at a maximum. At this point, the stored energy can be released by discharging the fluid/air to the non-working side of the device, thus resetting the un-stretched spring length, as shown in Figure 2a. This approach yields the 1-4 device behaviour of Figure 1b. Figure 2b shows a modified device design that treats each chamber independently [2]. This approach eliminates the need to rapidly dissipate energy between the two chambers, as in the coupled design of Figure 2a. The resulting independent control of the pressure and energy dissipation on each side of the piston for each portion of response motion allows greater flexibility in designing the overall device behaviour. This design thus enables a much broader range of control laws as each valve can be operated independently.

By utilising a common, well-understood fluid such as air, analyses and modelling of the device is made simpler [2]. Furthermore, by utilising air as the working fluid, the atmosphere can be used as the fluid reservoir, eliminating the need for complex external plumbing systems to reticulate the working fluid. There are several tradeoffs in the complexity of semi-active resetable devices when compared to electro-rheological or magneto-rheological smart dampers [12, 13]. The rheolgical dampers do not have valves, but their potentially large hysteretic behaviour and the lag introduced by it in slow response to inputs make control implementation more difficult.

A combination of the atmospheric fluid reservoir, for a pneumatic (air-based) device, and independent valve design allows more time for pressures to equalise during the valve reset, as resetting does not require the compressed working fluid to flow to the opposite chamber. While one chamber is under compression, the previously reset chamber can have the valve open for a

longer period to allow the pressure to equalise, as this valve does not affect the compression in the other chamber. This approach would not be feasible in the design shown in Figure 2a, as extending the valve reset time prevents the other chamber from storing energy. Thus, the newer device design in Figure 2b is more practicable than the former design in Figure 2a.

Modelling the device's force displacement characteristics uses the fundamental thermodynamic laws. Each chamber volume can be directly related to the device's piston displacement, which causes a change in pressure and generates the resisting force in the device. Resetting the device, by opening the valve of the compressed chamber, dissipates the stored energy as the chamber pressure equalises with the fluid reservoir, the atmosphere in the case of a pneumatic device. If the working fluid behaves as an ideal gas, and the compression is assumed to be reversible and adiabatic, then the ideal gas law can be utilised [3].

$$pV^{\gamma} = c \tag{1}$$

where γ is the ratio of specific heats, c is a constant and p and V are respectively the pressure and volume in a chamber of the device. Assuming the piston is centered and the initial chamber pressures are P_0 with initial volumes, V_0, the resisting force is a function of displacement, x:

$$F(x) = (p_2 - p_1)Ac = \left[(V_0 + Ax)^{-\gamma} - (V_0 - Ax)^{-\gamma}\right]Ac \tag{2}$$

Assuming small motions, Equation (2) can be linearised.

$$F(x) = -\frac{2A^2 \gamma P_0}{V_0} x \tag{3}$$

where A is the piston area. The effective stiffness of the resetable device is therefore defined:

$$k_1 = \frac{2A^2 \gamma P_0}{V_0} \tag{4}$$

Similar equations can be used to independently model the pressure-volume status of each chamber of the device in Figure 2b. Equation (4) can then be used to design a device to produce a set resisting force at a given displacement, or a set added stiffness. Since Equation (4) includes the device geometry in A and V it can be used to parameterise the design space [2].

The important difference between the control laws in Figures 1 b-d is that those that resist from peak to peak (Figure 1b) or from the zero position to a displacement peak (Figure 1c) are reset at a displacement peak where the velocity is zero. As such, the valve reset time is not an imperative design parameter. The control law that resists motion towards the centre and releases the stored energy by valve reset at the equilibrium position is doing so at a non-zero velocity. This approach makes the reset times much more important, and significantly differentiates these control laws.

A one-fifth scale pneumatic-based prototype device has been constructed to enable experimental testing and device characterisation. Experimental device characterisation has been performed for

the 1-3 and 2-4 control laws of Figures 1c-d. The ideal model of Equations (1)-(4) has been modified using experimental results to obtain a more realistic, non-linear device model [8]. Peak stiffness value varied from 185 kN/m to 236 kN/m, which are slightly lower than the design value of 250 kN/m. Differences were attributed to air loss due to valve flexibility, and inability to perfectly centre the piston. The dimensions of the prototype device are presented in Figure 3a, and the experimental results for this prototype are presented in Figures 3b-c, with peak force levels of approximately 20kN. This force level represents an internal cylinder pressure in the range of 600-700kPa. The valves utilised for the prototype are Buschjost solenoid actuated diaphragm valves, with a maximum operating pressure of 10bar. It is important to note that, for ease of implementation, the prototype is a pneumatic device, and a full-scale pneumatic device could easily produce resistive forces in the range of 100kN. Furthermore, the same approach can be extended to more viscous working fluids with much larger bulk modulus and thus deliver much higher resistive forces, in a similar, relatively small package.

Several iterations of testing and modification of the device model have provided theoretical and experimental force-displacement plots that match well. Figures 3b-c show these results for the control laws of Figures 1c-d, respectively. The hysteretic behaviour of the experimental device is very similar in shape to the idealised model, and magnitudes match well. Note that the major difference in the tensile portion of Figure 3b is due to loss of hydraulic test system pressure, with details in Mulligan et al [2, 8]. Based on these results, and to minimise the computational power required, the simpler idealised model of Equations (1)-(4) is used in developing the response spectra, with no anticipated loss of generality.

The frequency of experimental testing is important for practical implementation of resetable devices, and should be done at frequencies similar to those expected in earthquake induced structural vibrations. Therefore, Figure 4 shows the experimental results of a prototype device using the 1-3 control law at 1Hz and 2Hz for amplitudes of 16.5 and 10mm respectively. Larger amplitudes cannot be tested at higher frequencies due to limitations in the testing equipment, however the 1-2Hz frequencies in Figure 4 for relatively large amplitude motion is representative of trends in typical earthquake records. Note that the experimental results of Figure 4 correspond to a prototype device with shorter cylinder length to the one used to create Figure 3, and as such stiffness values and peak forces are different to the hysteresis loops presented in Figure 3.

Total system delays including sensing response, valve reset and energy dissipation are also an important practical consideration. The total delays in the system are shown in Figure 5a, which shows the load cell data and the valve control commands for an experimental test. Introducing a valve reset during a stroke shows the delays in the system from the time the valve reset command is given, to the time at which the drop in force occurs as a result of the valve reset. The enlarged view of the valve reset in Figure 5b indicates that the valve reset command is given at 14.664 seconds, and the force begins to drop at approximately 14.688 seconds. This results corresponds to a total delay between valve reset command and pressure drop of approximately 24ms, which is in the range of the valve reset times quoted with reference to the work of Barroso et al [4], and Hunt [1]. Furthermore, noting that the valve is closed again shortly after this reset, the total time between the first valve reset command (at 14.664s) and the start of the increase in force as the

valve is closed again (~14,71s) is less than 50ms. This time includes the lag between the valve opening command being sent, the valve opening, pressure equilibrating, the valve closure command being sent, the valve closing, and pressure again beginning to increase within the cylinder. Hence, there is a total cycle for two valve operations of 50ms, which offers significant speed relative to typical structural periods of 0.5-2.0 seconds.

3.0 Analysis Methods

This paper investigates the relative effectiveness of the three different control laws in Figures 1b-d by simulating the effect of the different valve control laws on the response of a seismically excited single degree of freedom structure fitted with a semi-active damper. The model structure includes internal structural damping of 5%. This value is commonly adopted by design codes and standards, is used in well-known textbooks [14], and has also been used in previous studies on damping systems [15]. The research utilises three earthquake suites from the SAC project [16], with 10 different time histories and two orthogonal directions for each history. The three suites represent ground motions having probabilities of exceedance of 50% in 50 years, 10% in 50 years, and 2% in 50 years in the Los Angeles region, and are referred to as the low, medium and high suites, respectively. Response statistics can thus be generated from the results of each probabilistically scaled suite.

Response spectra are generated for the three suites of ground motions, and spectral response plots were generated for the structural displacement, the structural force, the total base shear, and the area under the response spectra in a seismically important $T = 0.5 – 2.5$ sec range. The structural

force is defined as the base shear for a linear, un-damped structure, whereas the total base shear is defined as the sum of the structural force and the resisting forces from the semi-active resetable device. The structural force is thus an indication of the required column strength, and the base shear is an indication of the required foundation strength.

The reductions achieved by the addition of semi-active resetable devices are represented by reduction factors, normalised to the uncontrolled case results. These factors enable easy comparison of the different control laws and are a multiplicative factor. Each response spectra is generated from 0.1 to 5.0 seconds in 0.1 second increments. These spectra were created for each device type and devices of 50% and 100% stiffness, as compared to the stiffness of the single degree of freedom structure analysed.

Analysis of the results confirmed that the distribution of response outcomes can be well modeled by a log-normal probability density function. Thus, the spectra can be analysed using the appropriate lognormal statistics for each suite and for all ground motions together [17]. Variables within each ground motion suite may be represented by a median (the log-normal mean) and log-normal standard deviation [18], referred to herein as the dispersion factor (β). For a log-normal distribution of n samples x_i, the log-normal geometric mean (median) $\hat{x}$ is defined:

$$\hat{x} = \exp\left(\frac{1}{n}\sum_{i=1}^{n}\ln(x_i)\right) \tag{5}$$

Similarly, the log-normal-based standard deviation, or dispersion factor β is defined:

$$\beta = \sqrt{\frac{1}{n-1}\sum_{i=1}^{n}(\ln(x_i / \hat{x}))^2} \tag{6}$$

The statistical values used to indicate the change in response reduction factors are the median, or 50th percentile, in Equation (5), and dispersion factor of Equation (6). The first metric indicates the expected value of the response while the second indicates the relative spread (or dispersion) over the suite of ground motions. Utilising complete earthquake suites rather than individual earthquakes eliminates the likelihood of erroneous conclusions being drawn about the viability of a control law due to atypical performance for a single earthquake. Thus, the two statistical parameters ($\hat{x}$, β) are plotted against each natural period increment to investigate overall trends.

Finally, empirical equations are derived to approximate the reduction factors for a given amount of additional stiffness. These equations allow future applications of resetable devices to be extended to accepted structural design analysis methods. The systematic bias introduced by incorporating these empirical equations into structural design analysis is also investigated.

Although this investigation focuses on single degree of freedom (SDOF) systems, the use of semi-active resetable dampers can be easily extended for use in multiple degree of freedom (MDOF) structures with configurations using single and multiple devices for suites of probabilistically scaled ground motions [3, 4, 9, 19-21]. Specifically, research has shown that placing resetable devices in different configurations throughout the SAC3 structure with total

authority of approximately 2000kN, representing 13.8% of building weight, can provide geometric mean reductions in peak drift ranging from approximately 3-20%, and geometric mean reductions in permanent drift as large as 83.5% [4]. Further research could investigate the relative effects of the different resetable device control laws in MDOF structures. However, this study focuses on their analysis for inclusion in fundamental design methods.

4.0 Results and Discussion

Each earthquake record within a given suite was used to simulate the structural response and the maximum response value recorded for each period to generate the response spectra for every earthquake record at 0, 50, and 100% additional stiffness. The maximum structural force and maximum total base-shear was also recorded and normalised to the uncontrolled state to give reduction factors. Therefore, the multiplicative structural force reduction factors give an indication of the change in the demand on the columns, whereas the total base-shear reduction factors indicate the change in foundation demand.

4.1 Structural Force and Base Shear Results

The geometric mean structural force reduction factors for each suite are presented for the 1-3, 2-4, and 1-4 control laws in Figures 6a-c respectively. The results indicate that the reductions are largely independent of the suite used. Therefore, in Figure 6d, the structural force reduction factors are averaged across all three suites and plotted for all three device types. These overall average reduction factors indicate the relative ability of the different control laws at reducing the seismic demand on the columns. Figure 6d indicates that the 1-4 device is about twice as

effective as the 1-3 and 2-4 devices. Specifically, the reductions factors are approximately 0.65-0.8 for the 1-3 and 2-4 devices, which are very similar, and 0.4-0.5 for the 1-4 device. This result is expected as the 1-3 and 2-4 devices only operate over two quadrants, whereas the 1-4 device operates over all four quadrants, as shown in Figure 1. As such, the 1-3 and 2-4 devices provide resistive forces for a smaller percentage (~50%) of each cycle and will consequently have shorter active strokes, and thus store and dissipate less energy.

The total base-shear reduction factors for 100% additional stiffness were obtained at every period for each record and device type. As with the structural force, the geometric mean base-shear reduction factor for each suite is plotted against natural period for each control law in Figures 7a-c and the results averaged across all suites are given in Figure 7d. Figures 7a-c indicate the relative reduction in total base shear across the three earthquake suites, whereas Figure 7d indicates the relative ability of the three control laws at reducing the overturning demands on the foundation system. In this case, only the 2-4 device achieves significant reductions, with the 1-3 and 1-4 devices resulting in substantial increases across a majority of the spectrum. Again, the results indicate that the reductions achieved for each device are largely suite invariant.

4.2 Displacement Spectral Area Reduction Factors

The structural force and base-shear reduction factors were observed to be largely suite invariant and approximately constant within the natural period range of 0.5 to 2.5 seconds. The area under the displacement response spectra from structural period of 0.5 to 2.5 seconds is therefore examined as an indication of the magnitude of the response over this range. This range is a

critical region for earthquake resistant design, above which the predominant design factor is wind loading. The area under the displacement response spectra was numerically integrated for each earthquake and normalised to the uncontrolled case to give area reduction factors. The geometric mean of these area reduction factors was taken for each suite and then averaged across all three suites due to the previous results displaying invariance to the type of ground motion. This procedure was performed for the three control laws, with values of 0, 20, 50, 80, and 100% additional resetable device stiffness, as shown in Figure 8. These area reduction factors can be interpreted as an average reduction factor across the range of natural periods from 0.5 to 2.5 sec, representing a majority the constant velocity region of the spectra.

The area reduction factors in Figure 8 show similar reductions for the 1-3 and 2-4 control laws. Both the 1-3 and the 2-4 fall well short of the reductions achieved for the 1-4 control law, consistent with the other metrics. The reduction factors for the 1-3 and 2-4 control laws range from 1.0 to approximately 0.65 as the additional stiffness is increased from 0% to 100%, with the 2-4 control law slightly outperforming the 1-3 control law across the entire range. The 1-4 control law shows the greatest reduction in the displacement spectral areas, with a reduction factor of approximately 0.4 for 100% additional stiffness.

4.3 Empirical Area Reduction Factors

To extend resetable devices to design analysis, empirical equations are fitted to the results to approximate the reduction factors for a given percentage of additional resetable device stiffness. The area reduction factors calculated from the empirical equations are also plotted in Figure 8.

The form of the empirical equations is:

$$R = 1/B \tag{7}$$

where R is the multiplicative reduction factor, and B is the divisive reduction factor, defined as:

$$B = \sqrt{1 + C\frac{K_{resetable}}{K_{structural}}} \tag{8}$$

where $K_{resetable}$ is the additional stiffness provided by the resetable device, $K_{structural}$ is the structural stiffness, and C is a constant dependant on the control law, and has a value of 1.43, 1.59, and 5.75 for the 1-3, 2-4, and 1-4 control laws respectively.

Furthermore, the empirical reduction factors can be utilised to quantify the additional stiffness in terms of equivalent viscous damping, and compare the reductions achieved by the semi-active system to those that can be achieved by the use of a simple viscous damper. The overall effective damping can be represented by an intrinsic damping component, and a hysteretic damping component, defined as an equivalent viscous damping [15]. The intrinsic damping is the inherent structural damping, typically defined as 5% of critical for a spectral investigation and the hysteretic component can be defined as:

$$\xi_{eq} = \frac{C}{10}\frac{K_{resetable}}{K_{structural}} \tag{9}$$

where ξ_{eq} is the equivalent viscous damping of the added resetable device. Equation (9) can be used to show that 100% additional stiffness will produce 14.3%, 15.9%, and 57.5% equivalent viscous damping for the 1-3, 2-4 and 1-4 control laws respectively.

4.4 Displacement Reduction Factor Results

The maximum displacement response was recorded for every simulation to obtain the displacement spectra for every earthquake record and all three control laws at 0, 50 and 100% additional resetable stiffness. These displacement spectra are normalised to the uncontrolled case to obtain the displacement reduction factors at every natural period. These reduction factors are plotted against natural period, for the 1-3, 2-4, and 1-4 control laws at 50% and 100% added stiffness and presented in Figure 9. The reduction factor values given by Equations (7)-(8) are also plotted as horizontal lines in Figure 9, to graphically indicate how accurately these equations represent the actual displacement reduction factors. Although some variation from the empirical equation can be seen above T = 3.0 second period, Figure 9 shows that the empirical equations are appropriate over the entire constant velocity region of the spectra, between natural periods of 0.4 and 3.0 seconds.

To investigate the suite dependence of the reduction factors, the normalised reduction factors are calculated. These normalised reduction factors are defined as the geometric mean reduction factor derived from each suite divided by the overall geometric mean reduction factors from all ground motion records in all three suites. The normalised reduction factors give an indication of the relative performance of the semi-active resetable devices across each suite, where a value

close to 1.0 indicates little deviation from the overall average. The results from this analysis are presented in Figure 10, and show that the displacement reduction factors are largely suite invariant, with values close to unity for most periods, for all device types and stiffness values.

4.5 Analysis of Bias and Spread

To investigate the systematic bias introduced by the use of the empirical equations to approximate the displacement reduction factors, the multiplicative error factors are calculated. These factors are determined by dividing the actual reduction factor by the reduction factor from Equation (7), for the corresponding control law and additional stiffness, at every period. The results of this analysis are presented for all three control laws, at 50 and 100% additional stiffness, in Figure 11. The multiplicative error factors show that over the constant velocity region of T = 0.4-3.0 seconds the systematic bias introduced by the use of the empirical equations is generally less than ±20%, with the 2-4 control showing variations generally less than ±10%.

To give a further indication of the spread of the results, the dispersion factor, β, of the normalised displacement spectra are plotted in Figure 12 for each suite and device type at both 50% and 100% added stiffness. This figure gives an indication of the level of variation of these normalised average results, and indicates the consistency with which the different control laws can mitigate the response for a range of ground motion records. Dispersions (β) of the displacement reduction factors, shown in Figure 12, show that the 1-4 control law leads to noticeably larger record-to-record variability than the 1-3 and 2-4 devices. Over the typical range of use, dispersion factors in the order of β = 0.2-0.25 can be expected for the 1-3 and 2-4 control laws, whereas for the 1-4

damper this increases to β = 0.3-0.35. Again, the results are seen to be largely suite invariant.

5.0 Summary of Relative Performance

5.1 Performance of the 1-4 Control Law

Overall, the results show several, perhaps expected, phenomena. The 1-4 control law shows the biggest reduction in both displacement response and structural force. However, a possible shortfall of the 1-4 control law is that, on average, it results in only minimal reductions, and in many cases substantial increases, to the total base-shear force. This result is clearly evident in Figure 7, with reduction factors of approximately 0.9 at low structural natural periods, but at higher periods the reduction factors increase to approximately 1.6. This peak value represents a 60% increase in the total base shear and is a potentially undesirable result due to the increase in force and overturning demands on the foundation system. Such a result may be of little consequence for new, purpose designed structures, as the foundation can be strengthened to account for the use of a 1-4 device, which consequently lowers the demand on the columns during seismic events to minimise structural damage.

5.2 Performance of the 1-3 Control Law

Figure 7d shows similar trends in base shear demands for the 1-3 and 1-4 control laws with slightly larger increases for the 1-3 device across a majority of the spectrum. As with the 1-4 device, the peak reduction factor is 1.6 representing a 60% increase in foundation demand. Hence, the 1-3 device has the same undesirable impact as the 1-4 device with reductions in

displacement response coming at the expense of an increase in total base shear. More generally, it may be less desirable to semi-actively resist only motion away from equilibrium for these reasons.

5.3 Performance of the 2-4 Control Law

However, increased foundation loads would be of potentially high importance for retrofit applications where it is neither practical, nor feasible, to strengthen the foundations. Such retrofit applications are particularly important as a substantial majority of the built environment in 2025 has likely already been constructed. The 2-4 control law only resists motion *towards* the equilibrium position and releases energy at the equilibrium position. This approach is also very effective at reducing displacement response, as seen in Figure 9, with reduction factors of approximately 0.7-0.85, and 0.55-0.75 for 50 and 100% added stiffness respectively, similar to the 1-3 device. The spread of the results across the three suites in Figure 10 shows only minimal deviations across the spectrum with values close to 1.0. The 2-4 control law is the most consistent of the three control laws across all ground motion records, and indicates that the performance of the 2-4 device, in particular, is suite invariant and is equally appropriate for both the near field or far field ground motions described by these suites.

The significant advantage of the 2-4 control law over its counterparts is its ability to provide displacement and structural force reductions, while also reducing the total base-shear transmitted to the foundation, as seen in Figures 7a-d. These figures show that while the 1-3 and 1-4 control laws increase total base shear across almost the entire spectrum, the 2-4 control law reduces the

base shear across the same range of structural natural periods. This result is of particular interest if considering retrofit of semi-active resetable devices to existing buildings where it is not generally feasible to strengthen the foundation system to cope with the increased demand. More specifically, 2-4 resetable damping offers unique opportunities to add supplemental damping that are not readily available via more traditional, passive supplemental damping and retrofit devices.

Overall, the most applicable approach to sculpting hysteretic behaviour, by any means, depends on the critical design parameters. If the foundations can be strengthened appropriately, and the reduction in column demand is the critical parameter, then it is best to implement the 1-4 control law that resists all motion. However, if the strength of the foundation is limited, or important in a retrofit application, a 2-4 control law that resists only motion toward the centre is better. Finally, for any given percentage of additional stiffness the geometric mean or log-normal standard deviation of the results within each suite is not notably affected by the suite for any of the three control laws investigated.

6.0 Capacity Spectrum Implementation for Simplified Seismic Analysis and Design

The results of the analysis in design lend themselves towards use in the capacity spectrum method. The capacity spectrum method is useful where a realistic evaluation of the earthquake hazard can be analysed based on the statistical analysis of past earthquake records. The seismic demand spectrum is given as the lesser of:

$$C_d = \frac{F_a S_s}{B} \tag{9}$$

$$C_d = \frac{F_v S_1}{TB} \tag{10}$$

$$C_d = \frac{F_v S_1 T_d}{T^2 B} \tag{11}$$

where F_a and F_v are adjustments on spectral acceleration for short and long periods at different soil classes; S_s and S_1 are spectral acceleration at short periods and the one-second period; B is the approximate damping reduction factor defined in Equations (7)-(8); T = the period of the structure; and T_d = the period at the junction of the constant spectral velocity and displacement portions of the spectra. For convenience, setting the value of Design Acceleration Intensity to 1g, and assuming normal soil, then $F_v S_1$ = 1g, and setting $F_a S_s = 2.5 F_v S_1$ enables Equations (9)-(12) to be simplified to the lesser of: $C_d = 2.5/B$, $C_d = 1/TB$, and $C_d = T_d/T^2 B$. The customary code-based acceleration-period design spectra can be transformed into Acceleration-Displacement Response Spectra (ADRS) by using the following transformation:

$$\Delta = C_d T^2 \frac{g}{4\pi^2} \tag{12}$$

Thus Equations (10) and (11) respectively become:

$$\Delta = \left(\frac{F_v S_1}{B}\right)^2 \left(\frac{g}{4\pi^2}\right) \frac{1}{C_d} \tag{13}$$

$$\Delta = \left(\frac{F_v S_1}{B}\right) \left(\frac{g}{4\pi^2}\right) T_d \tag{14}$$

The corresponding ADRS are presented for the three control laws with 0, 20, 50, 80, and 100% additional resetable stiffness in Figure 13. These spectra show the largest reductions for the 1-4 control law due to the larger values of the reduction factors, *B*, matching the spectral analyses.

7.0 Conclusions

Overall, this research demonstrates that the novel new two chamber, resetable device design allows a broader range of control laws than conventional semi-active devices. These broader control laws provide the ability to semi-actively re-shape hysteretic behaviour to provide the most appropriate hysteresis loop for a given application. Based upon the investigation described herein, the following conclusions can be drawn:

- The hysteretic behaviour can be re-shaped to minimise structural force or minimise base-shear depending on design requirements.
- Analysis of displacement response and structural force indicate that all three device types reduce structural demand effectively. The 1-4 device achieves the highest reductions due to its longer active strokes and consequently higher energy absorption and dissipation, but is also the most variable over all three suites.
- All three control law devices are largely suite invariant indicating a robustness to the type of ground motion encountered.
- Displacement spectral area reduction factors showed substantial reductions achieved by the use of up to 100% additional stiffness, with similar results between the 1-3 and 2-4 devices. The largest reductions were again seen for the 1-4 device.

- The systematic bias introduced by use of empirical equations to the approximate the area reduction factors was generally less than 20%. The analysis is easily extended to the capacity spectrum method to incorporate resetable devices into future design analyses.
- A major distinction between the control laws is that the 2-4 device is the only device that reduces total base shear, as well as structural force and displacement response. These devices are unique in their ability to add damping only in the 2^{nd} and 4^{th} quadrants, and provide a unique opportunity for retrofit of structures with limited ability to manage increased base shear.
- The ability to actively re-shape hysteretic behaviour for given applications holds significant promise in the ability to mitigate seismic structural damage. Finally, it is important to note that it is not the exact reductions that are important, but rather the unique characteristics of the device types and their corresponding effect on structural response parameters.

Overall, the methods presented can be generalised as an effective analysis approach to other semi-active or passive devices. The resetable device control laws used can also be readily generalised to other working fluids or even to similar devices, such as viscous dampers. Most importantly, the approach presented is amenable to direct use in performance based design methods, increasing the ability to consider these devices and methods in more practical experiments.

References

[1] S. Hunt, "Semi-active smart-dampers and resetable actuators for multi-level seismic hazard mitigation of steel moment resisting frames," *Master of Engineering (ME) thesis, Dept of Mechanical Engineering, University of Canterbury, Christchurch, New Zealand.*, 2002.

[2] K. J. Mulligan, J. G. Chase, A. Gue, T. Alnot, G. W. Rodgers, J. B. Mander, R. B. Elliott, B. L. Deam, L. Cleeve, and D. Heaton, "Large Scale Resetable Devices for Multi-Level Seismic Hazard Mitigation of Structures," *Proc. 9th International Conference on Structural Safety and Reliability (ICOSSAR 2005), Rome, Italy, June 19-22.*, 2005.

[3] J. E. Bobrow, F. Jabbari, and K. Thai, "A New Approach to Shock Isolation and Vibration Suppression Using a Resetable Actuator," *ASME Transactions on Dynamic Systems, Measurement, and Control.*, vol. 122, pp. 570-573, 2000.

[4] L. R. Barroso, J. G. Chase, and S. Hunt, "Resettable smart dampers for multi-level seismic hazard mitigation of steel moment frames," *Journal of Structural Control*, vol. 10(1), pp. 41-58, 2003.

[5] L. M. Jansen and S. J. Dyke, "Semiactive Control Strategies for MR Dampers: Comparative Study," *ASCE Journal of Engineering Mechanics*, vol. 126(8), pp. 795-803, 2000.

[6] O. Yoshida and S. J. Dyke, "Seismic Control of a Nonlinear Benchmark Building Using Smart Dampers," *ASCE Journal of Engineering Mechanics*, vol. 130, pp. 386-392, 2004.

[7] F. Jabbari and J. E. Bobrow, "Vibration Suppression with a Resetable Device," *ASCE Journal of Engineering Mechanics*, vol. 128(9), pp. 916-924, 2002.

[8] K. Mulligan, J. Chase, A. Gue, J. Mander, T. Alnot, B. Deam, G. Rodgers, L. Cleeve, and D. Heaton, "Resetable Devices with Customised Performance for Semi-Active Seismic Hazard Mitigation of Structures," *Proc of NZ Society for Earthquake Engineering 2005 Conference (NZSEE 2005), March 11-13, Wairakei, New Zealand.*, 2005.

[9] J. G. Chase, L. Barroso, and S. Hunt, "The impact of total acceleration control for semi-active earthquake hazard mitigation," *Journal of Engineering Structures, Elsevier Science*, vol. 26(2), pp. 201-209, 2004.

[10] K. J. Mulligan, M. Fougere, J. B. Mander, J. G. Chase, B. Deam, G. Danton, and R. B. Elliott, "Semi-Active Rocking Wall Systems for Enhanced Seismic Energy Dissipation," *8th US National Conference on Earthquake Engineering (8NCEE), San Francisco, April 18-21, 10-pages.*, 2006.

[11] G. W. Rodgers, J. B. Mander, J. G. Chase, K. J. Mulligan, B. Deam, and A. J. Carr, "Re-Shaping Hysteretic Behaviour Using Resetable Devices to Customise Structural Response and Forces," *8th US National Conference on Earthquake Engineering (8NCEE), San Francisco, April 18-21, 10-pages.*, 2006.

[12] S. J. Dyke and B. F. Spencer, "Modeling and control of magnetorheological dampers for seismic response reduction," *Smart Materials and Structures*, vol. 5, pp. 565-575, 1996.

[13] B. F. Spencer, S. J. Dyke, M. K. Sain, and J. Carlson, "Phenomenological Model of Magnetorheological Damper," *ASCE Journal of Engineering Mechanics*, vol. 123, pp. 230-238, 1997.

[14] A. K. Chopra, "Dynamics of Structures : Theory and Applications to Earthquake Engineering," Prentice-Hall Inc, New Jersey, USA, 729pp, 1995.

[15] G. Pekcan, J. B. Mander, and S. S. Chen, "Fundamental Considerations for The Design of Non-linear Viscous Dampers," *Earthquake Engineering and Structural Dynamics*, vol. 28, pp. 1405-1425, 1999.

[16] P. Sommerville, N. Smith, S. Punyamurthula, and J. Sun, "Development of Ground Motion Time Histories For Phase II Of The FEMA/SAC Steel Project, SAC Background Document Report SAC/BD-97/04," 1997.

[17] R. P. Kennedy, C. A. Cornell, R. D. Campbell, S. Kaplan, and H. F. Perla, "Probabilistic Seismic Safety Study Of An Existing Nuclear Power Plant.," *Nuclear Engineering and Design*, vol. 59, pp. 315-338, 1980.

[18] E. Limpert, W. A. Stahel, and M. Abbt, "Log-normal distributions across the sciences: keys and clues.," *Bioscience 2001; vol 51(5), pp. 341-352.*, 2001.

[19] K. Mulligan, J. Chase, L. Barroso, and S. Hunt, "Impact of Control Architecture in the Reliability of Resetable Device Controlled Tall Structures," *Proc. 9th Intl Conf on Structural Safety and Reliability (ICOSSAR 2005) Rome, Italy, June 19-22, 8-pages, ISBN 90-5966-040-4.*, 2005.

[20] J. G. Chase, K. J. Mulligan, L. R. Barroso, and S. J. Hunt, "Actuator-Actuator Interaction and Instability in Decentralised Semi-Active Control of Non-Linear Seismically Excited Tall Structures,," *Proc. 9th International Conference on Structural Safety and Reliability (ICOSSAR 2005), Rome, Italy, June 19-22, 8-pages, ISBN 90-5966-040-4.*, 2005.

[21] J. G. Chase, L. Barroso, and S. Hunt, "Impact of Decentralized Semi-Active Control on the Stability of Tall Structures Under Seismic Loading,," *Proc. 2003 Pacific Earthquake Engineering Conference (PCEE), CD-ROM, 8 pages, Christchurch, NZ, February 13-15.*, 2003.

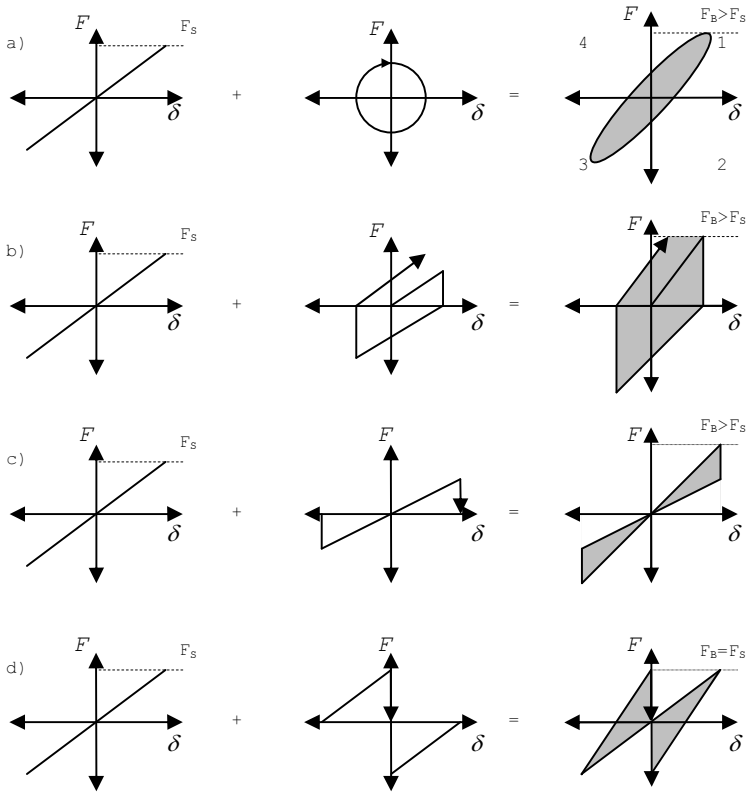

Figure 1: Schematic hysteresis for a) viscous damping, b) a 1-4 device, c) a 1-3 device, and d) a 2-4 device. Quadrants are labelled in the first panel, and F_B = total base shear, F_S = base shear for a linear, undamped structure. $F_B > F_S$ indicates an increase due to the additional damping.

a)

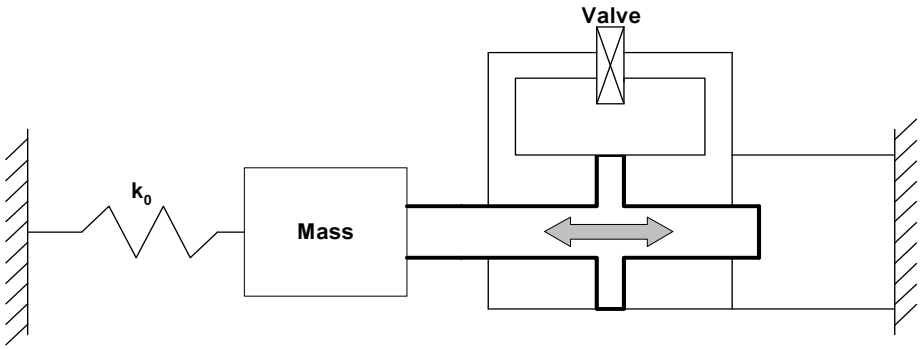

b)

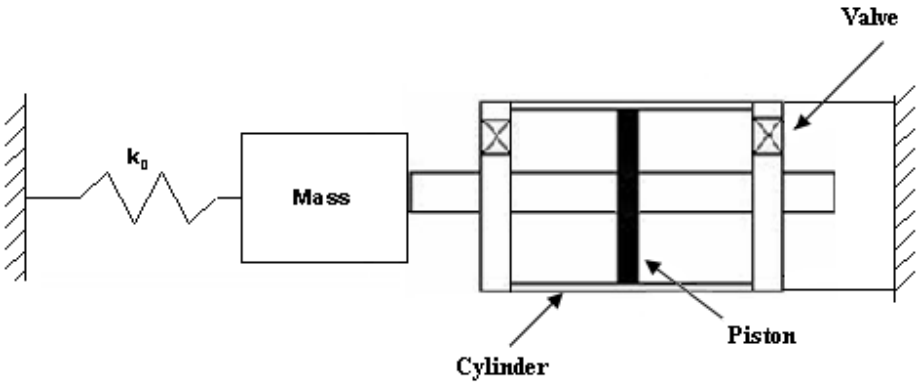

Figure 2: Schematic representation of semi-active devices attached to a single degree-of-freedom system a) Schematic of conventional resetable device using an external plumbing system with a single valve to connect the two sides of the piston. b) Schematic of independent chamber design. Each valve vents to atmosphere for a pneumatic, or air-based device.

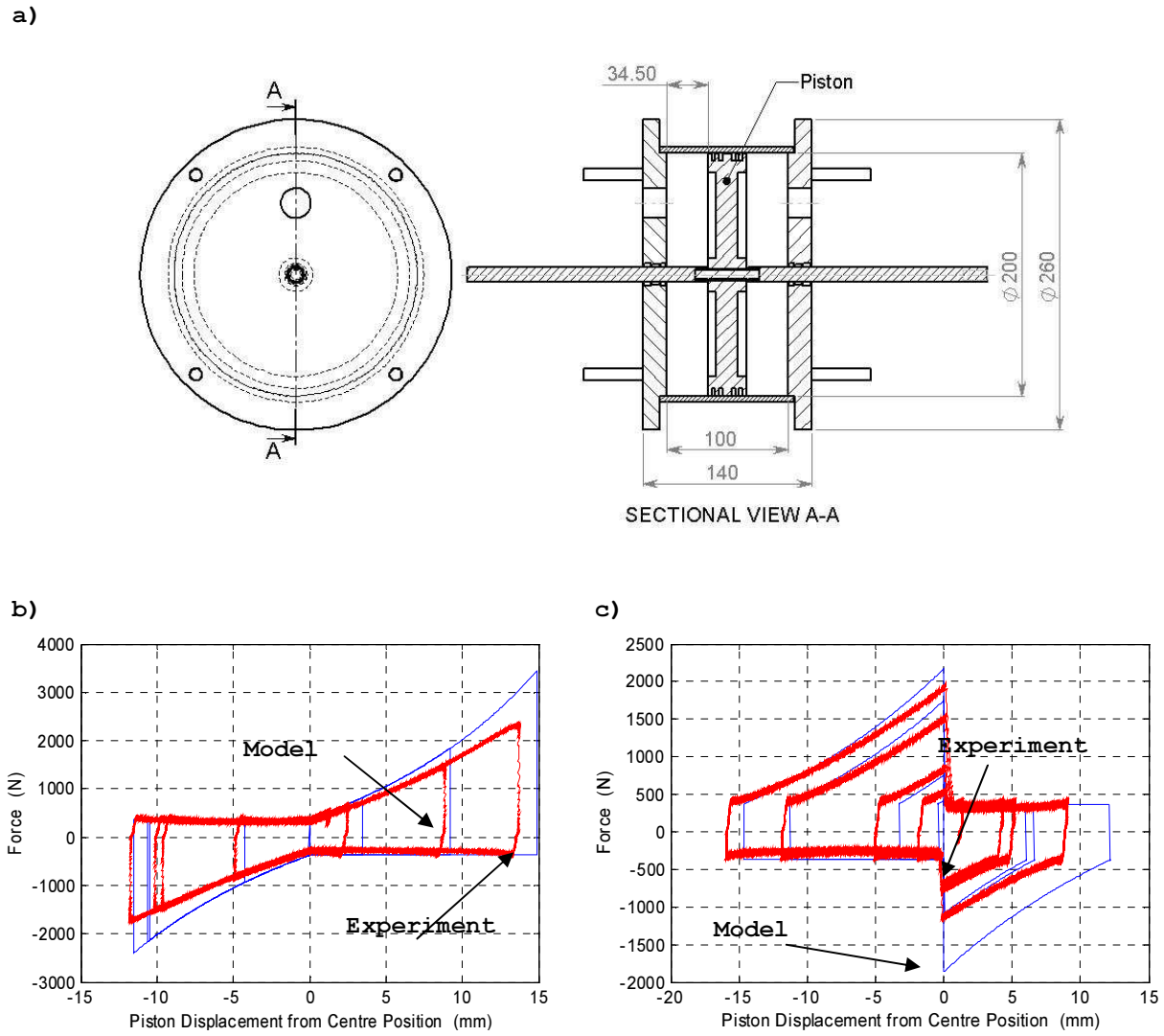

Figure 3: a) Dimensioned drawing of the prototype resetable device, and the Force-displacement curves for actuator in a single degree of freedom structure showing both the analytical model prediction and experimental result. Ground motion is a 2 m/s^2 sine wave of frequency 0.1Hz. Figure 3 b) shows a 1-3 control law, and Figure 3 c) shows a 2-4 control law.

a)

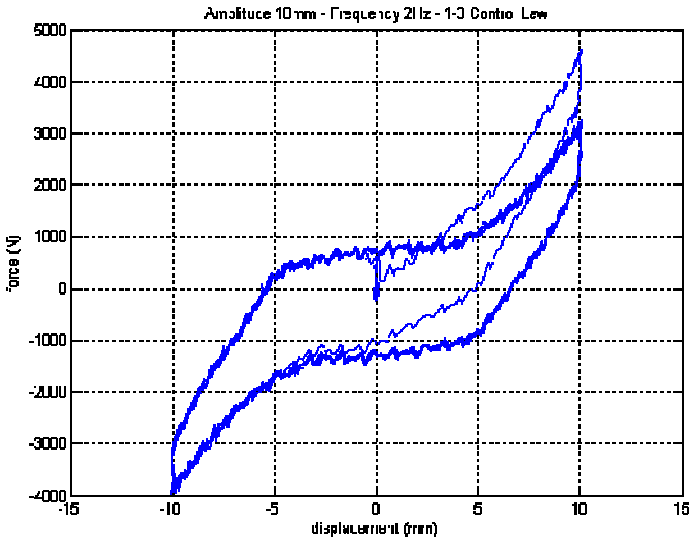

b)

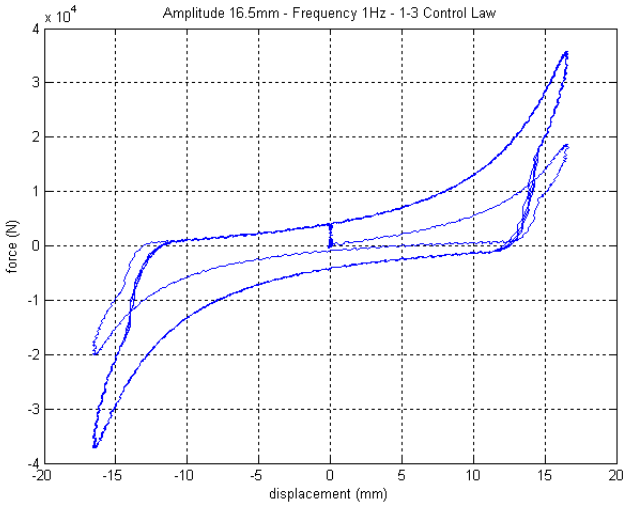

Figure 4: Experimental hysteresis loops for a prototype device tested with harmonic inputs of a) 10 mm amplitude and 2 Hz Frequency, and b) 16.5 mm amplitude and 1 Hz frequency.

a)

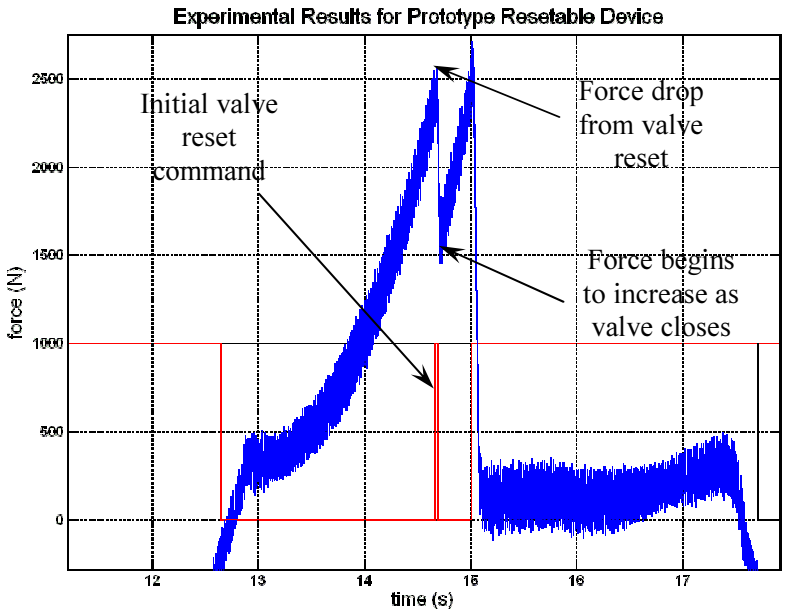

b)

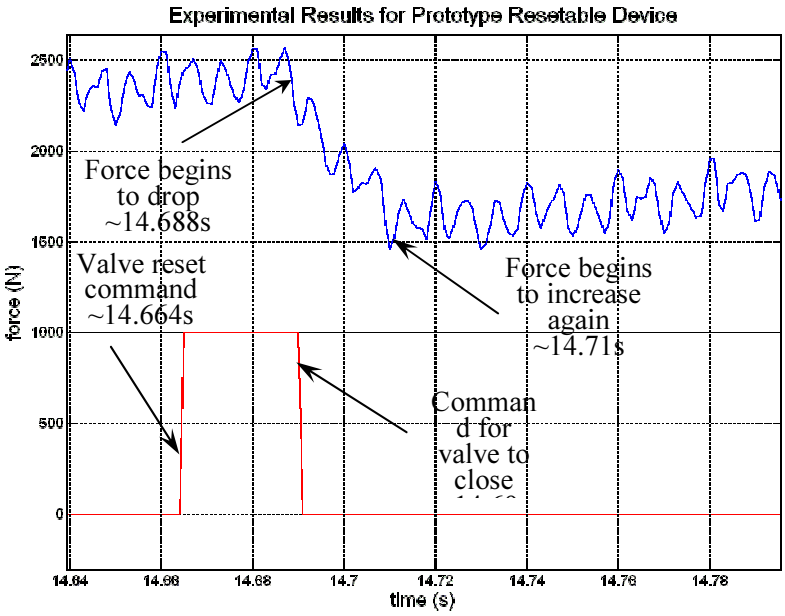

Figure 5: Total system delays shown by introducing a valve reset during compression, a) shows the overall force behaviour and b) shows an enlargement of the critical reset region.

a)

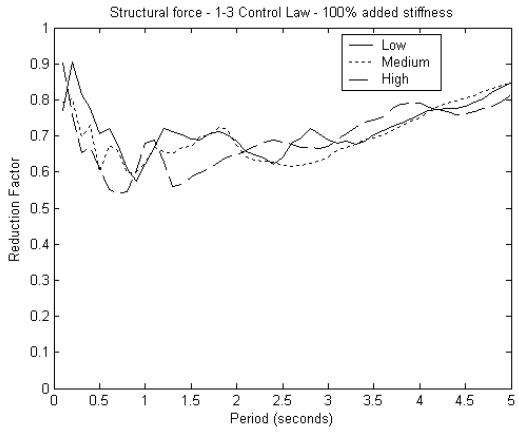

b)

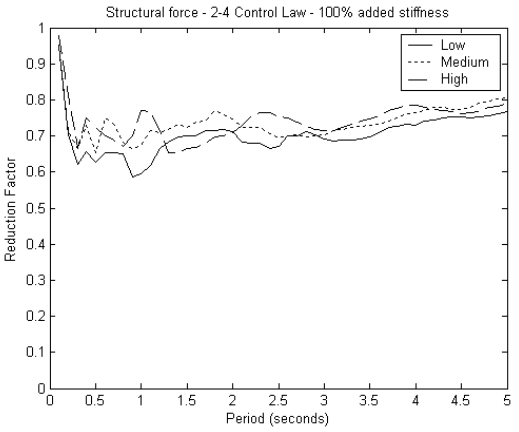

c)

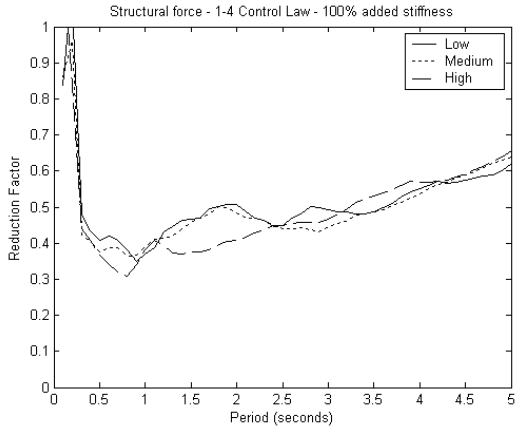

d)

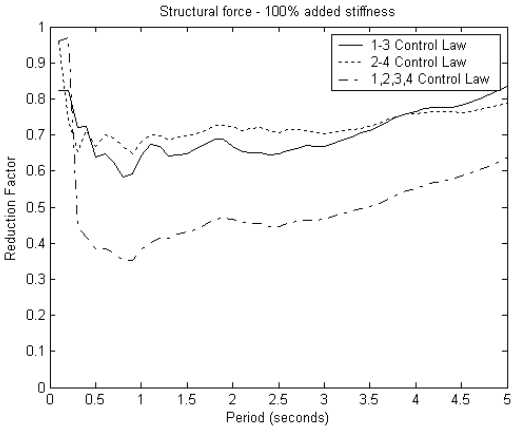

Figure 6: Reduction factors for the structural force for a linear, undamped structure, where (a-c) show each suite and device and (d) shows the three control laws averaged over all suites.

a)

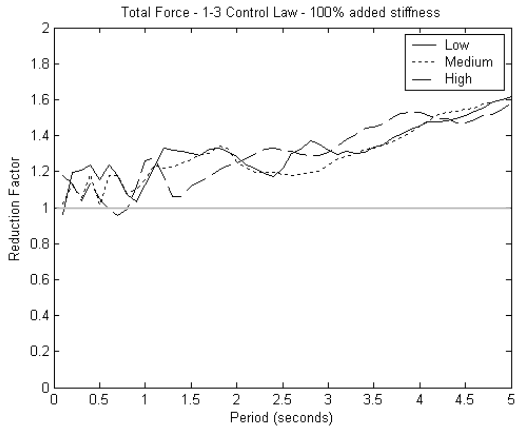

b)

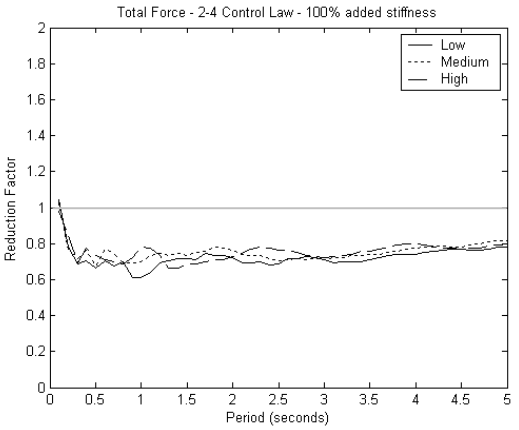

c)

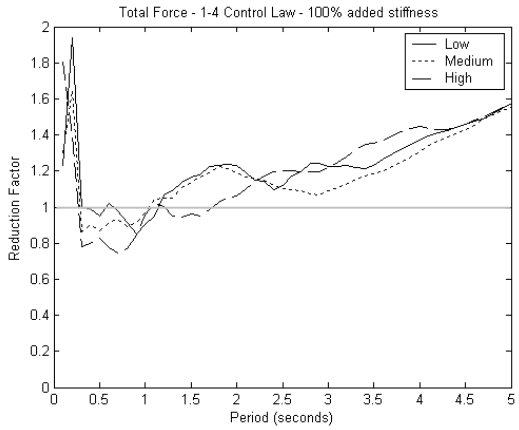

d)

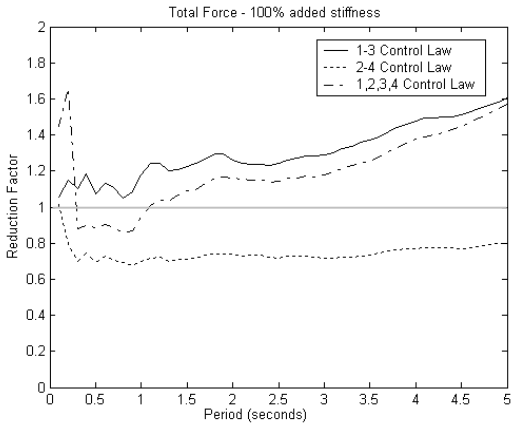

Figure 7: Reduction factors for the total base shear of a structure where (a-c) show the reduction factors for each suite and device, and (d) shows the averages across all suites for each device.

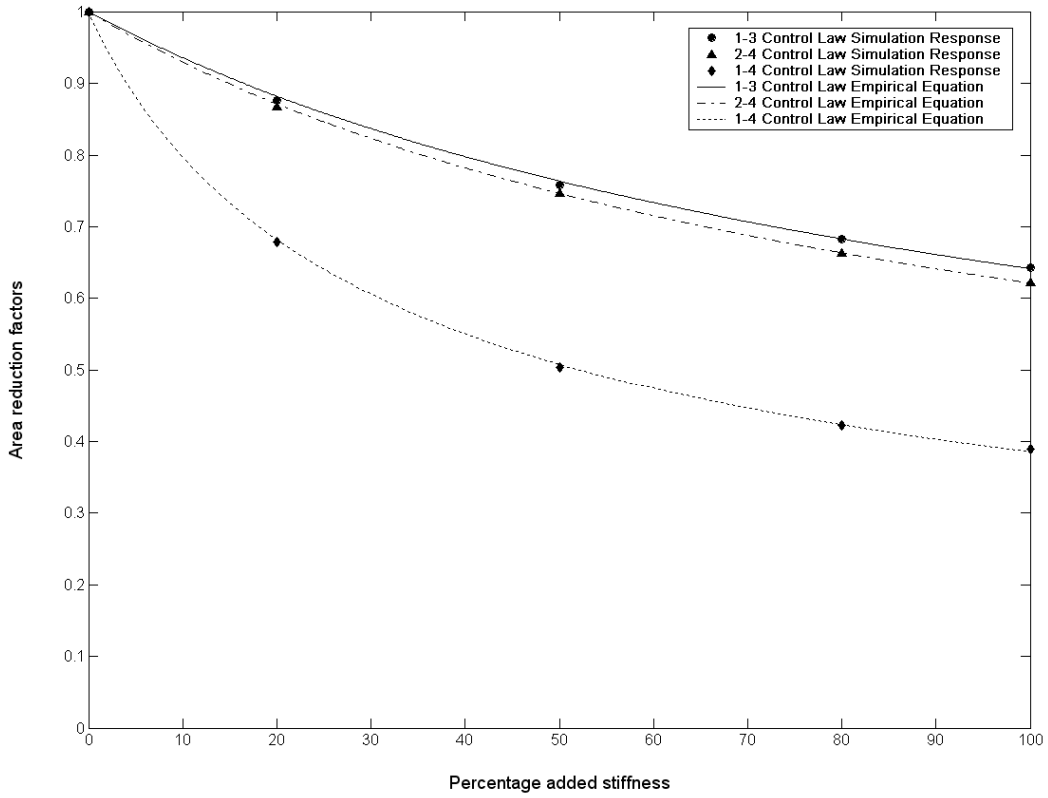

Figure 8: Reduction factors for the area under the displacement response spectra between 0.5 and 2.5 second periods normalised to the uncontrolled case and averaged across all suites.

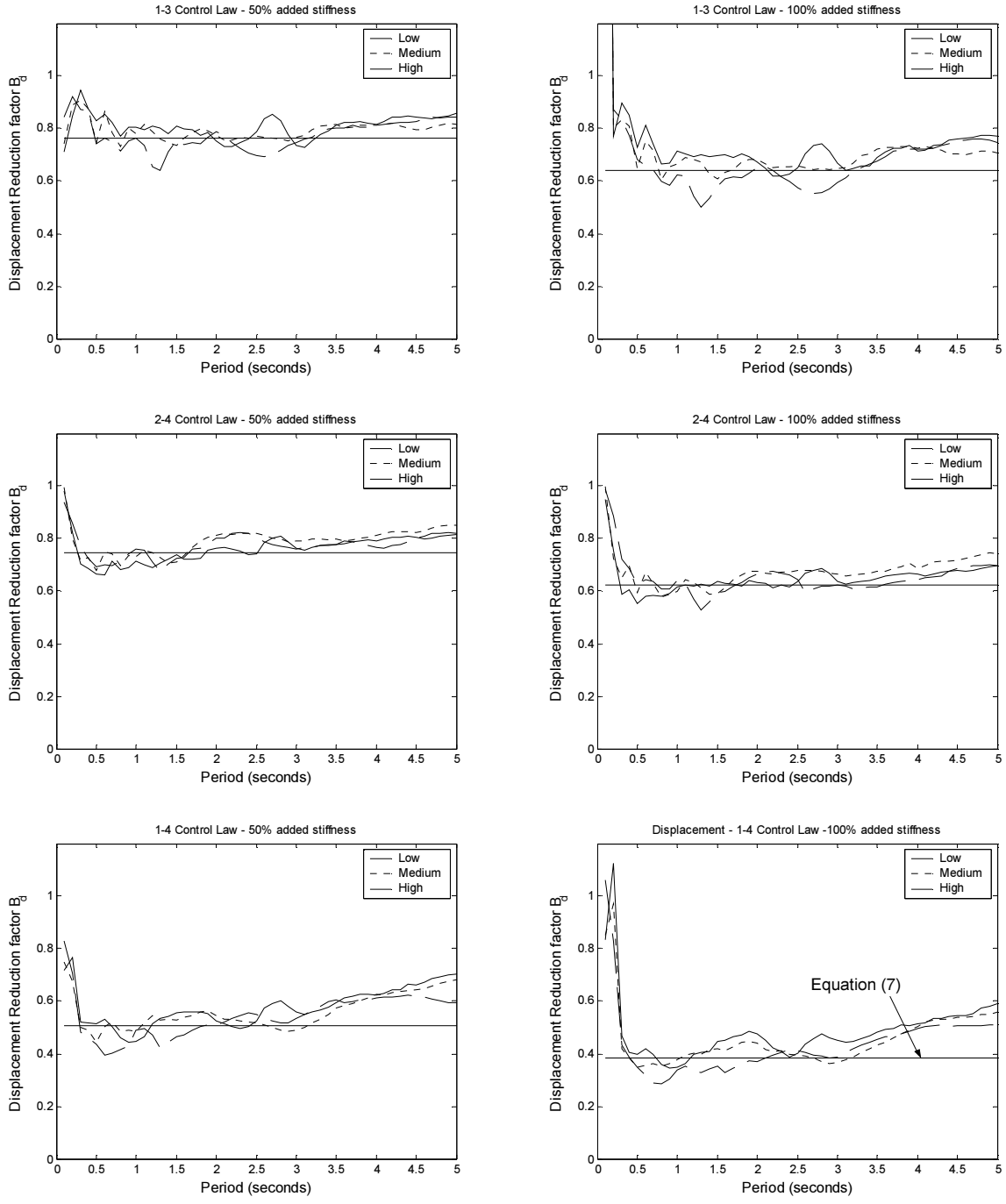

Figure 9: Displacement Reduction Factors for 50% and 100% added stiffness for all three control laws. Also shown are the reduction factors given by Equation (7).

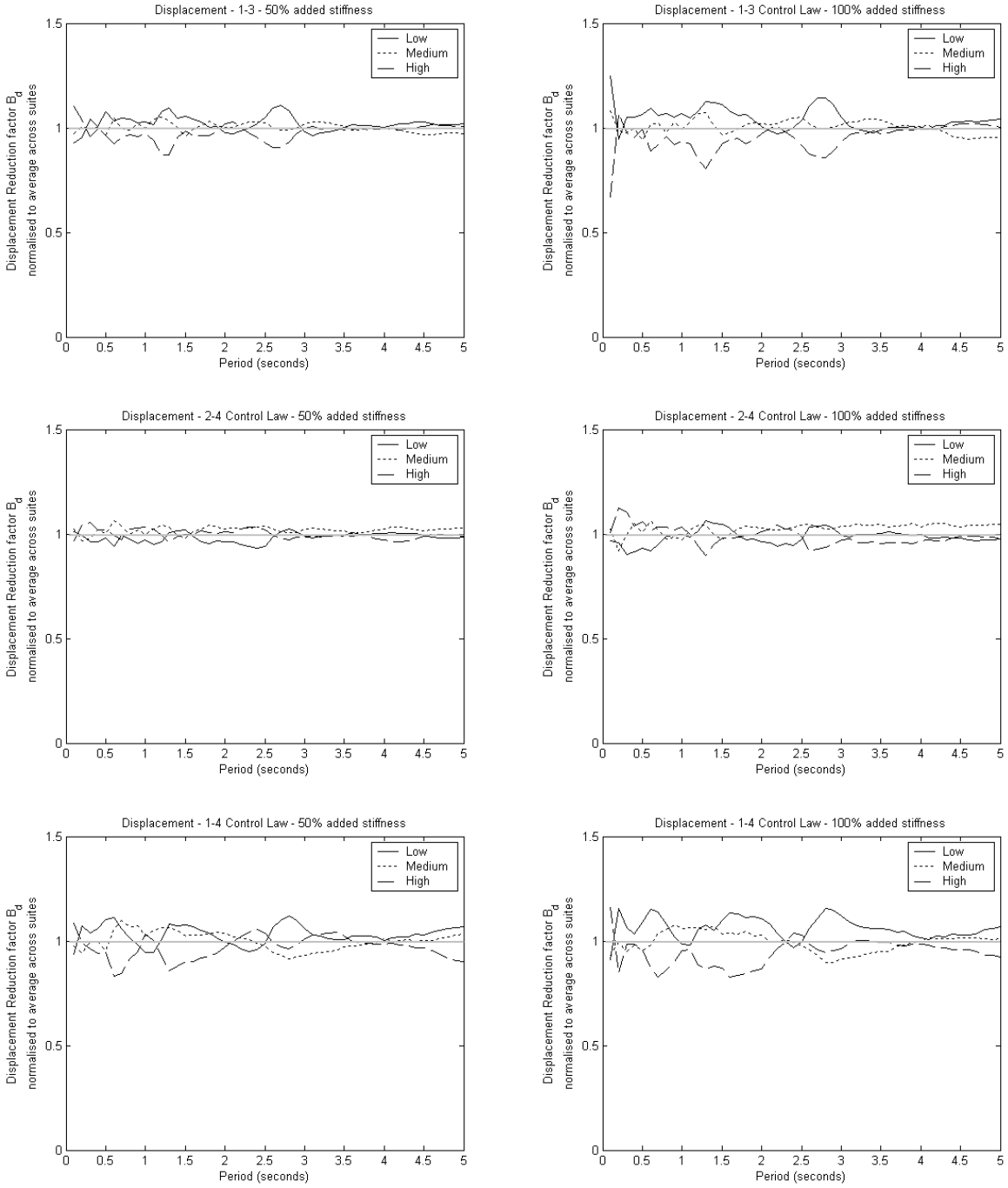

Figure 10: Displacement Reduction Factors for each suite normalised to the average value across all ground motion records for 50% and 100% added stiffness, for 1-3, 2-4 and 1-4 control laws.

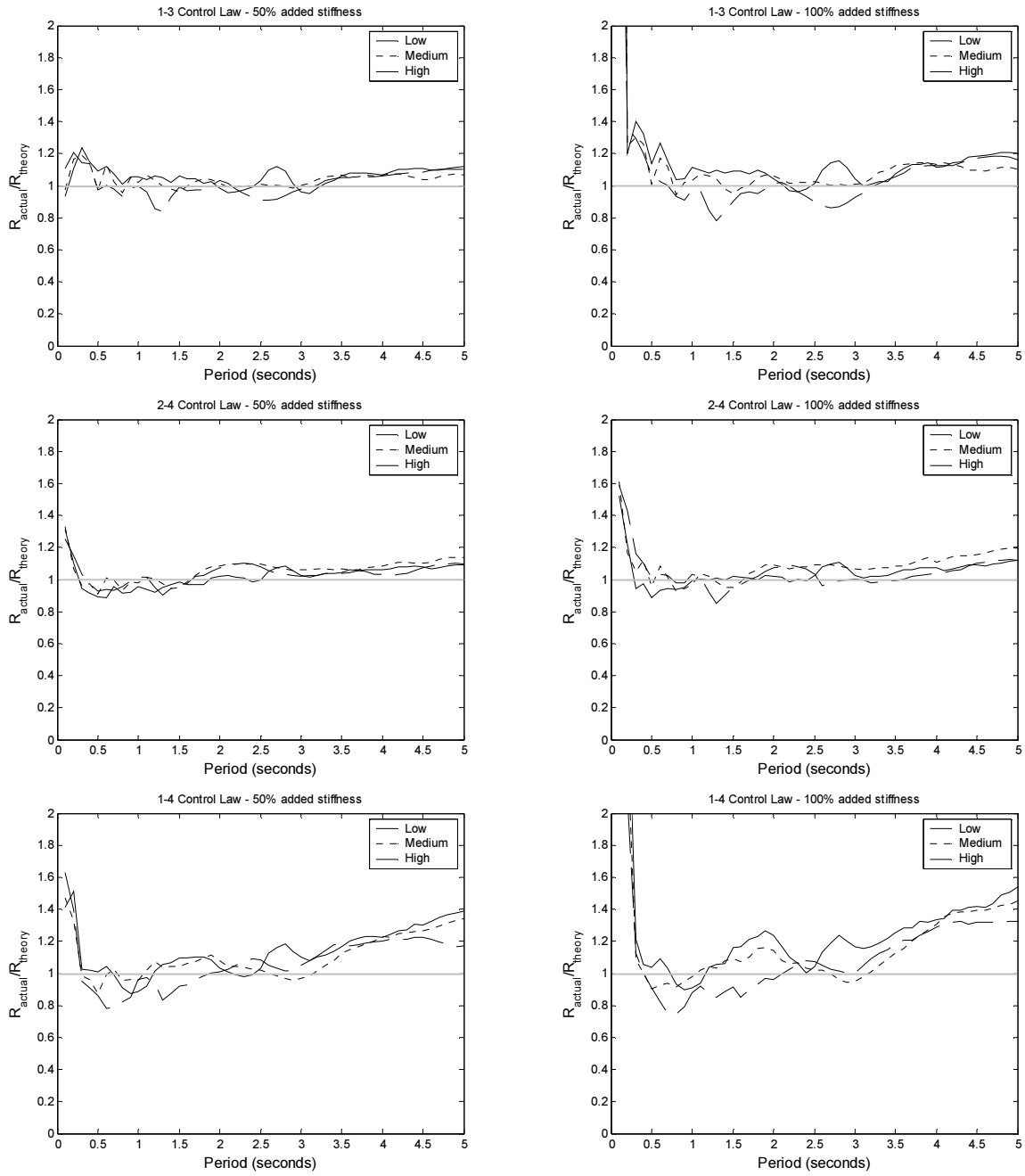

Figure 11: Displacement reduction factors normalized to the theoretical value given by Equation (7).

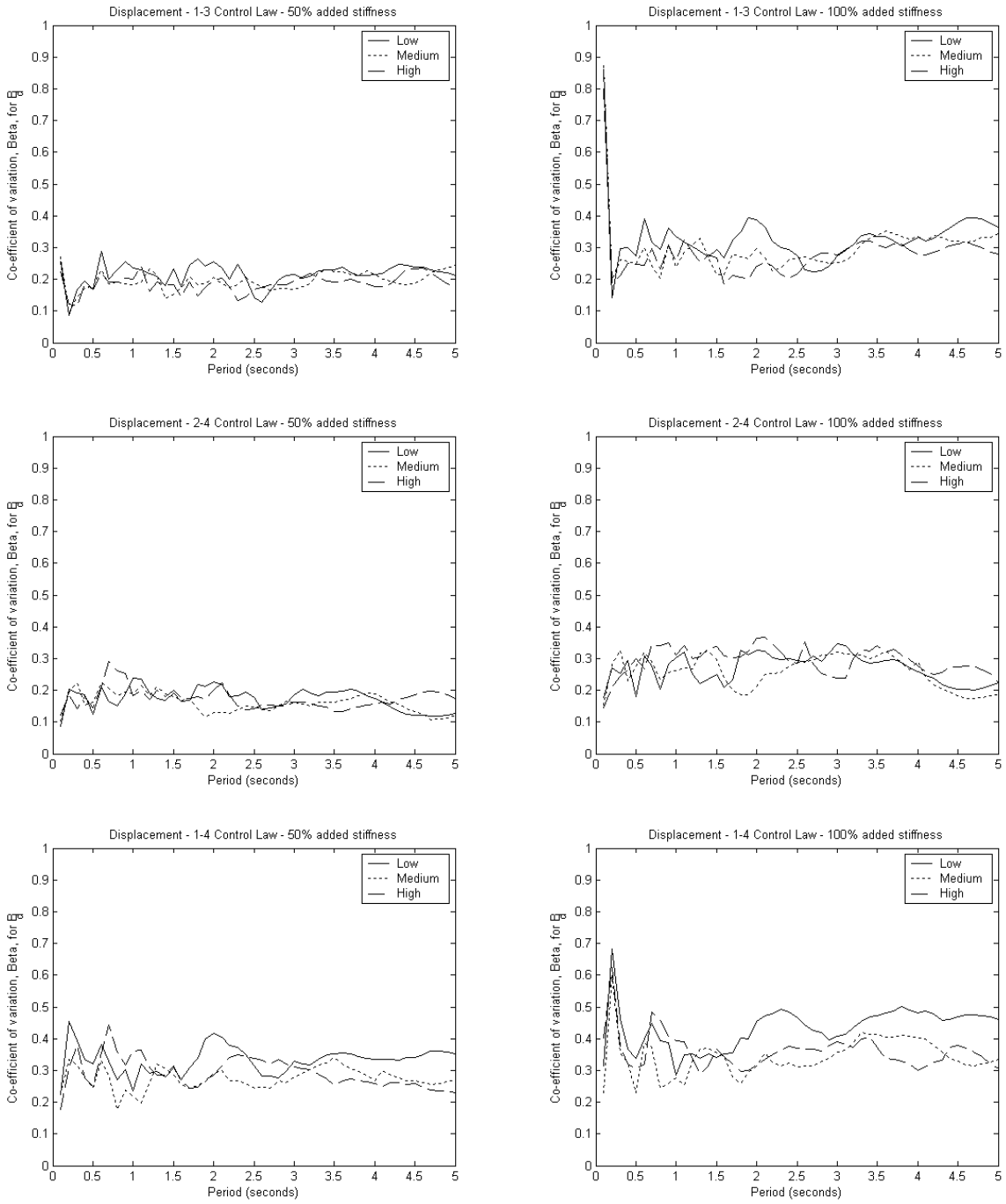

Figure 12: Coefficients of variation, β, for the displacement reduction factors.

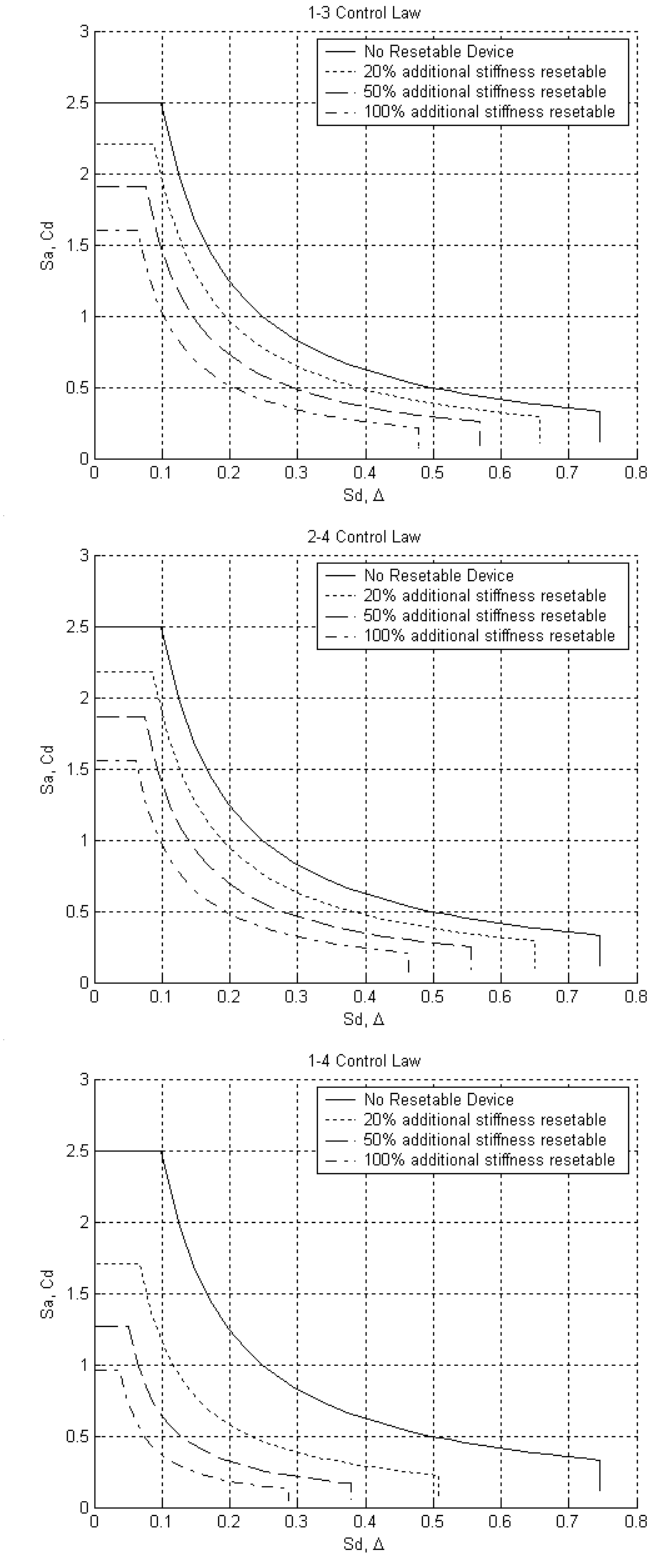

Figure 13: Acceleration Displacement Response Spectra (ADRS) for the three control laws.